PHILOSOPHICAL TRANSACTIONS OF THE ROYAL SOCIETY A MATHEMATICAL, PHYSICAL & ENGINEERING SCIENCES

Properties of Cross-Well Chaos in an Impacting System

Steven W. Shaw, Alan G. Haddow and Shang-Rou Hsieh

Phil. Trans. R. Soc. Lond. A 1994 **347**, 391-410
doi: 10.1098/rsta.1994.0050

Properties of cross-well chaos in an impacting system

By Steven W. Shaw[1], Alan G. Haddow[2] and Shang-Rou Hsieh[1]

[1] *Department of Mechanical Engineering and Applied Mechanics, The University of Michigan, Ann Arbor, MI 48109-2125, U.S.A.*

[2] *Department of Mechanical Engineering, Michigan State University, East Lansing, MI 48824-1226, U.S.A.*

In this paper we present results on chaotic motions in a periodically forced impacting system which is analogous to the version of Duffing's equation with negative linear stiffness. Our focus is on the prediction and manipulation of the cross-well chaos in this system. First, we develop a general method for determining parameter conditions under which homoclinic tangles exist, which is a necessary condition for cross-well chaos to occur. We then show how one may manipulate higher harmonics of the excitation in order to affect the range of excitation amplitudes over which fractal basin boundaries between the two potential wells exist. We also experimentally investigate the threshold for cross-well chaos and compare the results with the theoretical results. Second, we consider the rate at which the system crosses from one potential well to the other during a chaotic motion and relate this to the rate of phase space flux in a Poincaré map defined in terms of impact parameters. Results from simulations and experiments are compared with a simple theory based on phase space transport ideas, and a predictive scheme for estimating the rate of crossings under different parameter conditions is presented. The main conclusions of the paper are the following: (1) higher harmonics can be used with some effectiveness to extend the region of deterministic basin boundaries (in terms of the amplitude of excitation) but their effect on steady-state chaos is unreliable; (2) the rate at which the system executes cross-well excursions is related in a direct manner to the rate of phase space flux of the system as measured by the area of a *turnstile lobe* in the Poincaré map. These results indicate some of the ways in which the chaotic properties of this system, and possibly others such as Duffing's equation, are influenced by various system and input parameters. The main tools of analysis are a special version of Melnikov's method, adapted for this piecewise-linear system, and ideas of phase space transport.

1. Introduction and background

It is known that the source of chaos in many periodically forced oscillators is the occurrence of homoclinic tangles in which the stable and unstable manifolds of a saddle type periodic motion intersect (see, for example, Guckenheimer & Holmes 1986). These tangles do not imply the existence of *strange attractors* but generally act like chaotic saddle points, since almost all solutions can escape the tangle region. While near the tangle, such a motion will undergo transient chaos (Grebogi *et al.* 1983) and exhibit sensitive dependence on initial conditions and fractal basin

Phil. Trans. R. Soc. Lond. A (1994) **347**, 391–410
Printed in Great Britain

boundaries between any competing attractors (Moon 1992). When no basin of attraction of a stable periodic solution exists nearby, these tangles can dominate the dynamics, resulting in sustained, i.e. *steady-state* chaos.

Melnikov's method is an asymptotic method which can, in certain classes of systems (those with multiple potential wells), be used to estimate the parameter conditions at which these tangles appear (see Wiggins 1990 for a detailed exposition of the method). Neither it nor any known method can predict when a strange attractor may appear, but it does give a lower bound below which cross-well chaos cannot occur. (See Moon (1992) and the recent works of Szemplinska-Stupnicka (1992) and McRobie & Thompson (1993) for heuristic methods for determining conditions for the onset of sustained chaos.) In this sense, Moon (1992) describes homoclinic tangles as a precursor to sustained chaos.

When studying chaos in forced oscillators, by far the most common excitation used consists of a single harmonic input. However, as was mentioned in his original paper (Melnikov 1963), Melnikov's method is applicable for general periodic inputs. In the first part of the present study we use a special version of the method in order to determine parameter conditions for which homoclinic tangles exist for the system of interest. This method, due to the piecewise-linear nature of the system being considered, is exact and not asymptotic. It is used to demonstrate how higher harmonics can be manipulated in order to enhance or suppress the occurrence of homoclinic tangles. We also demonstrate that the method provides a very good estimate of the parameter conditions at which sustained cross-well chaos appears in the experimental version of the impacting system considered here.

Much recent work has been done using the ideas of phase space transport in order to describe the details of the dynamics in the tangle. This work is relevant to a wide variety of topics including fluid mixing (Ottino 1989) and escape from potential wells (McRobie & Thompson 1990). One of the key ideas in this work is that the rate at which volumes of phase space are transported from one region of phase space to another, i.e. the *rate of phase space flux*, is related to the volumes of certain key 'lobes', called turnstiles, whose boundaries are composed of pieces of the stable and unstable manifolds in the tangle. Melnikov's method can be used to estimate the area of these turnstiles in an asymptotic manner for small excitation and damping levels. Wiggins (1992) contains detailed descriptions of these notions and many examples. In this work we show that the rate of phase space flux, as measured by the turnstile area, is directly related to the rate at which the system undergoes cross-well transitions. The results are confirmed using simulations and physical experiments, and a predictive method is developed based on the theory.

The remainder of this paper is organized as follows. We first describe the system which is being considered, give its equations of motion and briefly describe the experimental apparatus. (This is a generalization of the system considered in Shaw & Rand (1989) and Moore & Shaw (1990).) In §3 we describe the general ideas behind the manipulation of the homoclinic tangle using harmonics in the excitation and present the attendant calculations for generating some optimal types of inputs. We also show experimental results that demonstrate the effectiveness of Melnikov's method in predicting the point at which sustained cross-well chaos appears for this system. In §4 we present a brief account of the ideas of phase space flux, their application to the system at hand and provide results obtained from simulations and experiments. The paper closes with a discussion in §5 and further information about the experimental apparatus is provided in the Appendix.

2. The impacting system

The physical system considered here is depicted in figure 1. Analytical and experimental results for this system can be found in Shaw & Rand (1989) and Moore & Shaw (1990), respectively, for the case of a single harmonic input. An extension to a two degrees of freedom system is given in Shaw & Shaw (1989).

The pendulum pivot in figure 1 is centred between the two rigid upright barriers and the base is given a prescribed displacement of $s(\tau)$ where τ is time. The equations of motion for this system are

$$\left.\begin{aligned} ml^2\theta'' + b\theta' - mgl\sin\theta = ml\cos(\theta)\,s'', \quad & |\theta| < \theta_{\max}, \\ \theta' \to -r\theta', \quad & |\theta| = \theta_{\max}, \end{aligned}\right\} \tag{1}$$

where m and l are the mass of the pendulum bob and the length of the pendulum, respectively, b is the equivalent viscous damping coefficient for free-flight motions, g is gravitational acceleration, r is the coefficient of restitution for the impacts and a prime denotes a derivative with respect to τ. The value of $\theta_{\max}$ is the maximum allowable angular displacement ($\pm$); it is given by $\arcsin(d/2l)$, where d is the separation between the barriers. The base motion is taken to be periodic and written in Fourier series form,

$$s(\tau) = \sum_{j=1}^{\infty} A_j \sin(j\omega_{\mathrm{dr}}\tau + \psi_j), \tag{2}$$

where ω_{dr} is the base frequency of the excitation, A_j and ψ_j are the amplitude and phase of the jth harmonic, respectively, and we take $\psi_1 = 0$ without loss of generality. The barriers are assumed to be close together compared with the pendulum length, and therefore the linearized version of the equation of motion is valid for free flight between the barriers, so that $\theta_{\max} \sim d/2l$. The equation of motion is normalized by defining the normalized pendulum angle $x = \theta/\theta_{\max}$, the dimensionless time $t = \tau\sqrt{(g/l)}$, the damping ratio $\delta = b/(2ml\sqrt{(lg)})$, the non-dimensional driving frequency $\omega = \omega_{\mathrm{dr}}/\sqrt{(g/l)}$ and the dimensionless acceleration harmonic amplitudes $\gamma_j = -A_j j^2\omega_{\mathrm{dr}}^2/(g\theta_{\max})$. This rescaling, and linearization, result in the following equation of motion:

$$\left.\begin{aligned} \ddot{x} + 2\delta\dot{x} - x = \sum_{j=1}^{\infty} \gamma_j \sin(j\omega t + \psi_j), \quad & |x| < 1, \\ \dot{x} \to -r\dot{x}, \quad & |x| = 1. \end{aligned}\right\} \tag{3}$$

It will be convenient to sometimes denote the first harmonic acceleration amplitude as $\beta = \gamma_1$ and the period of excitation, $2\pi/\omega$, as T. We have written the input directly in terms of acceleration amplitudes for each harmonic, since these, rather than displacement amplitudes, are measured in the experiments.

More details of the physical apparatus can be found in the Appendix. However, the essential numerical values for the system parameters are $l = 253$ mm, $d = 33$ mm and thus $\theta_{\max} = 7.49°$, well within the region valid for linearization. The coefficient of restitution was measured directly from impacts and was found to be $r = 0.9$. (This value did depend on the impact velocity but stayed in a range of 0.85–0.95.) The free flight equivalent viscous damping coefficient was measured by the log-decrement method for the non-inverted pendulum and was determined to be $\delta = 0.03$. (This represents an average value since, due to nonlinear effects, δ varied in the range 0.025–0.035 for various amplitudes of oscillation.)

PHILOSOPHICAL TRANSACTIONS OF THE ROYAL SOCIETY A MATHEMATICAL, PHYSICAL & ENGINEERING SCIENCES

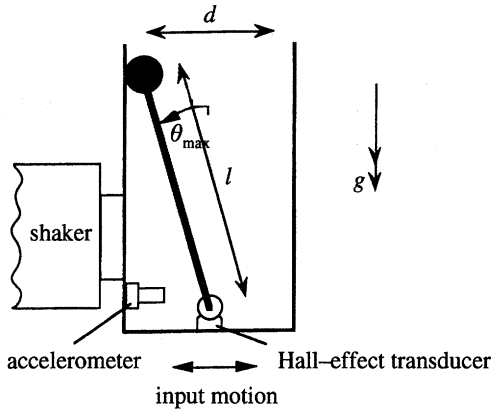

Figure 1. A schematic diagram of the physical device.

This system is qualitatively the same as Duffing's equation with negative linear stiffness. The unforced system has an unstable central equilibrium position ($x = 0$) with two symmetrically placed stable equilibria ($x = \pm 1$) and is provided with dissipation and subjected to periodic excitation. In the present case the nonlinearity is confined to the impact, whereas the usual Duffing equation has a cubic term in x which keeps the motion bounded. Dozens of papers have been written about the dynamics of Duffing's equation; see Guckenheimer & Holmes (1986) or Moon (1992) for some of the relevant references.

One interesting feature of this system which is distinct from Duffing's equation is that the equilibria ($x = \pm 1$), in which the pendulum rests against a barrier, persist for base motions with peak accelerations less than unity (in non-dimensional form). These trivial 'motions' are quite robust for small values of peak acceleration, and they can coexist with a variety of non-trivial motions, including chaos (see Moore & Shaw 1990 for more details). This has a direct bearing on the range of parameters for which experiments on the non-trivial dynamics can be carried out.

3. The onset of chaos

(a) *Analysis and simulations*

In this section we derive the critical parameter conditions for which homoclinic tangles appear for this system, with an emphasis on the effects of adding higher harmonics to the input. Our formulation is based on the assumption that the physical system is specified, that is, the damping, inertial and geometrical parameters are fixed.

The following derivation of the Melnikov function for this system is a generalization of the calculation found in Shaw & Rand (1989). Equation (3) possesses a saddle type periodic solution, $\gamma(t)\,(=\gamma(t+T))$, which emanates from the $x = 0$ equilibrium as the excitation is raised from zero. This solution represents a motion in which the pendulum performs a dynamic balancing act, wavering between the barriers in such a manner that the excitation keeps it from falling onto a barrier. Such a solution is clearly unstable. In the three-dimensional extended phase space $E = (x, \dot{x}, t(\mathrm{mod}\, T))$, $\gamma(t)$ is represented by a closed loop, and it appears as saddle type fixed point in the usual Poincaré map which samples $(x, \dot{x})$ once per period of the excitation. In $E, \gamma(t)$ has two-dimensional stable and unstable manifolds, $W^{\mathrm{s}}(\gamma(t))$

and $W^{u}(\gamma(t))$, respectively, which represent those points in E which approach $\gamma(t)$ as $t \to +\infty$ and $-\infty$, respectively. If these manifolds do not intersect, then motions coming near $\gamma(t)$ wil be repelled to one side ($x = +1$ or $x = -1$), never to return near to $\gamma(t)$, thus rendering the motion forever trapped on one side of the potential barrier. If these manifolds intersect, however, then there exists the possibility for motions which repeatedly return near to $\gamma(t)$ and make regular or irregular excursions from side to side; these include the cross-well chaotic motions which result from the existence of the homoclinic tangle.

The forms of these manifolds depend on the system and excitation parameters and, as they are changed, the manifolds can undergo global bifurcations in which they intersect (or separate, respectively), creating (or destroying, respectively) homoclinic tangles. Melnikov's method provides an oriented measure of separation of these manifolds in a subset of E and therefore it can be used as a predictive tool in determining parameter conditions at which this 'precursor' to chaos appears.

For the present system, since it is linear between the barriers, $\gamma(t)$ can be obtained without approximation for all parameter values for which $\max_{t\in[0,T)} \gamma(t) \leqslant 1$. Specifically, $\gamma(t)$ is simply given by the particular solution of equation (3), which is

$$\left.\begin{aligned} \gamma(t) = x_p(t) &= \sum_{j=1}^{\infty} \frac{\gamma_j}{\Gamma_j} \sin(j\omega t + \psi_j + \phi_j), \\ \Gamma_j &= \sqrt{[(1+(j\omega)^2)^2 + (2\delta j\omega)^2]}, \\ \tan(\phi_j) &= 2\delta j\omega/[1+(j\omega)^2], \quad \pi \leqslant \phi_j \leqslant \tfrac{3}{2}\pi, \end{aligned}\right\} \tag{4}$$

so long as $\max_{t\in[0,T)} x_p(t) \leqslant 1$ (i.e. it cannot penetrate a barrier). This solution is of saddle type stability, as can be inferred directly since the homogeneous solution of (3) is of the form

$$x_h(t) = C_1 e^{s_1(t-t_0)} + C_2 e^{s_2(t-t_0)}, \quad s_{1,2} = -\delta \pm \sqrt{(1+\delta^2)}, \tag{5}$$

and is composed of stable ($s_2 < 0$) and unstable ($s_1 > 0$) components. For initial conditions given by $(1, \dot{x}_0, t_0)$, the constants in x_h are given by

$$\left.\begin{aligned} C_1 &= [-s_2(1-x_p(t_0)) + \dot{x}_0 - \dot{x}_p(t_0)]/2\sqrt{(1+\delta^2)}, \\ C_2 &= [s_1(1-x_p(t_0)) - \dot{x}_0 + \dot{x}_p(t_0)]/2\sqrt{(1+\delta^2)}. \end{aligned}\right\} \tag{6}$$

These will be used in the development below.

The first pieces of $W^{s}(\gamma(t))$ and $W^{u}(\gamma(t))$ that intersect $x = +1$ in E (that is, those that emanate from $\gamma(t)$ directly to the barrier at $x = +1$) can be computed explicitly as follows. A surface of section which is natural to define in this case is

$$\Sigma = \{(x, \dot{x}, t(\mathrm{mod}\, T)) : x = +1, \dot{x} > 0\}, \tag{7}$$

which represents states in which the pendulum bob is just coming in contact with the barrier at $x = +1$ with positive velocity. (This is in contrast with the usual Poincaré section which is taken at a fixed phase of the excitation. This surface generates a Poincaré map which can be used for detailed analysis of periodic solutions and their stability; see Shaw & Rand 1989.) One piece of $W^{s,u}(\gamma(t)) \cap \Sigma$ can be determined by computing the conditions under which points at $x = +1$ are forward (for $W^{s}(\gamma(t))$) and backward (for $W^{u}(\gamma(t))$) asymptotic to $\gamma(t)$. These are found by setting $C_{1,2}$ in turn equal to zero.

We first determine those points in Σ which approach $\gamma(t)$ as $t \to -\infty$ without undergoing further impact, i.e. those in the first branch of $W^{u}(\gamma(t)) \cap \Sigma$. These are

denoted by $\dot{x}^{\mathrm{u}}(t_0)$, and are a set of $(\dot{x}, t_0)$ points which are parameterized by letting t_0 range from 0 to T. They are found by noting that in order for $\lim_{t\to-\infty} x(t) = x_p(t)$, then $\lim_{t\to-\infty} x_h(t) = 0$ must hold since $x = x_h + x_p$. This condition requires that $C_2 = 0$, since $\lim_{t\to-\infty} \mathrm{e}^{s_2(t-t_0)} = \infty$ by virtue of the fact that $s_2 < 0$. (Note that $\lim_{t\to-\infty} \mathrm{e}^{s_1(t-t_0)} = 0$ as required, since $s_1 > 0$.) The condition $C_2 = 0$ yields, directly from (6),

$$\dot{x}^{\mathrm{u}}(t_0) = s_1(1 - x_p(t_0)) + \dot{x}_p(t_0). \tag{8}$$

A similar argument shows that points in the first branch of $W^{\mathrm{s}}(\gamma(t)) \cap \Sigma$ are determined by setting $C_1 = 0$, to force $x(t)$ towards $x_p(t)$ as $t \to +\infty$. There is a twist in this case, since the first points in W^{s} to reach $x = +1$ have negative velocity, $\dot{x} < 0$. To bring them into Σ, the inverse of the impact rule is applied, that is, the points are multiplied by $-1/r$. This gives the points in Σ which, after an impact occurs, will then undergo free flight dynamics which are asymptotic to $\gamma(t)$. The procedure yields

$$\dot{x}^{\mathrm{s}}(t_0) = [-s_2(1 - x_p(t_0)) - \dot{x}_p(t_0)]/r. \tag{9}$$

We can now directly determine the separation of the manifolds in Σ by computing the separation function

$$\begin{aligned} d(t_0) &= \dot{x}^{\mathrm{u}}(t_0) - \dot{x}^{\mathrm{s}}(t_0) \\ &= [(s_1 r + s_2)(1 - x_p(t_0)) + (1 + r)\dot{x}_p(t_0)]/r. \end{aligned} \tag{10}$$

Note that $d(t_0) > 0$ (< 0, respectively) implies that $\dot{x}^{\mathrm{u}}(t_0)$ is above (below, respectively) $\dot{x}^{\mathrm{s}}(t_0)$ in Σ. Therefore, if $d(t_0)$ remains bounded away from zero, then the manifolds do not intersect, while if $d(t_0)$ crosses zero, the manifolds intersect.

Restrictions must be placed on the system parameters in order for the above expressions for $\dot{x}^{\mathrm{u}}(t_0)$, $\dot{x}^{\mathrm{s}}(t_0)$ and $d(t_0)$ to be valid. Specifically, $(\beta, \omega, r, \delta)$ must be such that $\dot{x}^{\mathrm{u}}(t_0)$ and $\dot{x}^{\mathrm{s}}(t_0)$ are both positive for $t_0 \in [0, T)$, so that they lie in Σ. This is the case for the parameter values used in the present study. In cases where $\dot{x}^{\mathrm{u}}(t_0)$ and/or $\dot{x}^{\mathrm{s}}(t_0)$ are negative over some t_0 range, the structure of the first branches of $W^{\mathrm{u}}(\gamma(t)) \cap \Sigma$ and/or $W^{\mathrm{s}}(\gamma(t)) \cap \Sigma$ are more complicated and not expressible in such simple terms.

Substitution of the Fourier series representation of $x_p(t)$ given in (4) and some trigonometric manipulations result in the following expression for $d(t_0)$:

$$\left.\begin{aligned} d(t_0) &= \tfrac{1}{2}D_0 + \sum_{j=1}^{\infty} D_j \sin(j\omega t + \psi_j + \phi_j + \nu_j), \\ D_0 &= 2(rs_1 + s_2)/r, \quad D_j = \gamma_j \Lambda_j/(r\Gamma_j), \\ \Lambda_j &= \sqrt{[(1+r)^2 (j\omega)^2 + (s_1 r + s_2)^2]}, \\ \tan(\nu_j) &= (1+r) j\omega/[-(s_1 r + s_2)], \quad 0 \leqslant \nu_j \leqslant \tfrac{1}{2}\pi, \end{aligned}\right\} \tag{11}$$

for $j = 1, 2, \ldots$, with $\gamma_1 = \beta$ and $\psi_1 = 0$. In a usual Melnikov analysis, this separation function is determined in an asymptotic form for small damping and forcing levels. In the present case, it is given exactly for all parameter values for which $|x_p| < 1$, $\forall t \in [0, T)$.

This function, $d(t_0)$, oscillates about a mean value of $\frac{1}{2}D_0$ (< 0) and has period T in t_0. As parameter values are varied, the point at which $d(t_0)$ develops zeros at some values(s) of t_0, with $d(t_0)$ negative everywhere else, corresponds to a global bifurcation in which homoclinic tangles are created.

It is interesting to consider the manner in which the input and output harmonics are related. This can be viewed as an input–output process which takes input amplitudes γ_j into output amplitudes D_j and gives a phase shift of $\phi_j+\nu_j$. The ratio D_j/γ_j is defined by the function $\lambda_j(\omega)$ given by

$$\lambda_j(\omega) = D_j/\gamma_j = \Lambda_j/(r\Gamma_j). \tag{12}$$

This function has the following properties: $\lambda_j(0) = (s_1 r+s_2)/r$ and for large ω, $\lambda_j(\omega) \approx (1+r)/(rj\omega)$.

We now consider a class of problems in which the system and the first harmonic are specified and it is assumed that a homoclinic tangle exists. The following question is considered: If one has access to all higher order harmonics, that is, all those for $j = 2, 3, \ldots$, can one select the (γ_j, ψ_j) in order to untangle the manifolds? In order to determine the widest parameter range for which this is possible, our goal is to minimize the peak value of $d(t_0)$. The solution to this problem is to provide an input, if feasible, which generates a square wave for $d(t_0)$, which has a fixed first harmonic (Axler 1988). In order for $d(t_0)$ to be a square wave, say of amplitude A, we must have $D_1 = 4A/\pi$, which gives $A = \pi D_1/4$ where D_1 is set by *fixed* parameters. For a square wave, the higher harmonics will be of odd order only and they must be in phase with the first. In order to achieve this, we force the term inside of the jth sine function to be equal to $j(\omega t+\phi_1+\nu_1)$. This implies that the excitation harmonics must have phases of

$$\hat{\psi}_j = j(\phi_1+\nu_1)-(\phi_j+\nu_j). \tag{13}$$

The amplitudes of the higher harmonics of a square wave are given by

$$D_j = \begin{cases} 4A/(j\pi) = D_1/j = \beta\Lambda_1/(rj\Gamma_1), & j = 3, 5, \ldots, \\ 0, & j = 2, 4, \ldots. \end{cases} \tag{14}$$

The required input amplitudes are obtained by equating the expressions for D_j given in (11) and (14). The result is

$$\hat{\gamma}_j = \begin{cases} \beta\Lambda_1\Gamma_j/(j\Gamma_1\Lambda_j), & j = 3, 5, \ldots, \\ 0, & j = 2, 4, \ldots. \end{cases} \tag{15}$$

The desired input is now completely specified in terms of fixed parameters. For such an input to be feasible, the corresponding Fourier series must converge. A simple estimate indicates that $\lim_{j,\,\mathrm{odd}\to\infty} \hat{\gamma}_j = (\beta\omega\Lambda_1)/((1+r)\Gamma_1)$, which is a non-zero constant, implying that the series does not converge. Therefore, there does not exist a realizable acceleration input which gives $d(t_0)$ the form of a square wave.

A more feasible and more easily achievable solution is to use only one (or some small number) of higher harmonics. In general, it is clear that even order harmonics are of no help whatsoever since, by their very nature, they cannot uniformly decrease $d(t_0)$ near its peak value. Here we use only the third harmonic and determine the optimal values for this case. First, the phase is chosen to be

$$\bar{\psi}_3 = \hat{\psi}_3 = 3(\phi_1+\nu_1)-(\phi_3+\nu_3), \tag{16}$$

to synchronize the first and third harmonics in $d(t_0)$. This reduces the problem to solving

$$\left.\begin{aligned} \bar{\gamma}_3 &= \min_{\gamma_3} \max_{t_0\in[0,\,T)} \tilde{d}(T_0), \\ \tilde{d}(T_0) &= \beta\lambda_1(\omega)\sin(T_0)+\gamma_3\lambda_3(\omega)\sin(3T_0), \end{aligned}\right\} \tag{17}$$

where $\tilde{d}$ is the oscillating part of d and $T_0 = \omega t_0 + \phi_1 + \nu_1$. This is solved as follows. Local extrema of $\tilde{d}(T_0)$ occur at

$$\bar{T}_{0,1,2,3\pm} = \tfrac{1}{2}\pi, \tfrac{3}{2}\pi, \sin^{-1}(\pm\sqrt{[\tfrac{1}{4} + \tfrac{1}{12}\beta\lambda_1/(\gamma_3\lambda_3)]}). \tag{18}$$

The first two solutions are the continuation of the extrema of the base sine wave which persist as extrema when the third harmonic is added exactly in or exactly out of phase. The latter solutions occur in pairs and exist only for $-\frac{1}{15} < \gamma_3\lambda_3/(\beta\lambda_1) < \frac{1}{9}$. These are the ranges over which the base sine wave develops 'dimples' in place of the original extrema, adding four new extrema, one pair straddling each of the original extrema. The extrema corresponding to the roots in (18) are given by

$$\tilde{d}(\bar{T}_{0,1,2,3\pm}) = (\beta\lambda_1 - \gamma_3\lambda_3), (-\beta\lambda_1 + \gamma_3\lambda_3), \pm(\tfrac{1}{3}(\beta\lambda_1 + 3\gamma_3\lambda_3)^{\frac{3}{2}}/\sqrt{(3\gamma_3\lambda_3)}). \tag{19}$$

The latter solutions are the ones of interest and can be minimized by taking the derivative with respect to γ_3, setting this equal to zero, and solving. The resulting equation has roots $\gamma_3 = -\beta\lambda_1/3\lambda_3$, $\beta\lambda_1/6\lambda_3$, of which the second is the desired solution, since an out of phase harmonic for sine functions will always increase the magnitudes of the peaks at $T_{0,1} = \frac{1}{2}\pi$ and $T_{0,2} = \frac{3}{2}\pi$. Therefore,

$$\bar{\gamma}_3 = \beta\lambda_1/6\lambda_3 = \beta\Lambda_1\Gamma_3/(6\Gamma_1\Lambda_3) \tag{20}$$

which yields the optimal input of

$$\beta\left[\sin(\omega t) + \frac{\Lambda_1\Gamma_3}{6\Gamma_1\Lambda_3}\sin(3\omega t + \bar{\psi}_3)\right]. \tag{21}$$

To determine the effectiveness of this added harmonic, we compare the threshold for tangles, that is the global bifurcation condition, for the original single harmonic input with that for the two harmonic inputs. The bifurcation occurs at points where the peak value of $d(t_0)$ is zero, implying a tangent zero. For the single harmonic case this occurs at an excitation amplitude such that the peak value of the oscillating part of $d(t_0)$ is equal to the magnitude of the direct current (DC) term, or, for this case, $D_1 = \frac{1}{2}|D_0|$, which gives

$$\beta_{\mathrm{cr}} = |\tfrac{1}{2}D_0 r\Gamma_1/\Lambda_1| = |\tfrac{1}{2}D_0/\lambda_1|. \tag{22}$$

The same calculation for the case with the added third harmonic requires the peak value of the oscillating part, which is given by $\tilde{d}(\bar{T}_{0,3\pm})$ with $\gamma_3 = \bar{\gamma}_3$. Setting this equal to $\frac{1}{2}|D_0|$ yields the critical condition in terms of the first harmonic amplitude

$$\beta^*_{\mathrm{cr}} = |D_0 r\Gamma_1/(\sqrt{3}\Lambda_1)| = |D_0/(\sqrt{3}\lambda_1)| \tag{23}$$

Thus, the value of β for which homoclinic tangles do not occur can be extended by a factor of $2/\sqrt{3} \approx 1.155$.

It is interesting to note that if one simply takes the third harmonic from the square wave solution as the only added harmonic, the resulting criterion is

$$\beta^{**}_{\mathrm{cr}} = |3D_0/[(3\sqrt{2}+1)\lambda_1]| \tag{24}$$

which is within 1% of the optimal solution for the single added harmonic.

Figure 2 shows plots of β_{cr} and β^*_{cr} against ω for $r = 0.9$ and $\delta = 0.03$, the experimental values. It is important to note that for ω values below approximately 10, the critical values are below unity, implying that homoclinic tangles occur while the rest positions are still stable. For this reason most of the experiments and simulations were run at relatively high frequencies at which the basins of attraction

PHILOSOPHICAL TRANSACTIONS OF THE ROYAL SOCIETY A MATHEMATICAL, PHYSICAL & ENGINEERING SCIENCES

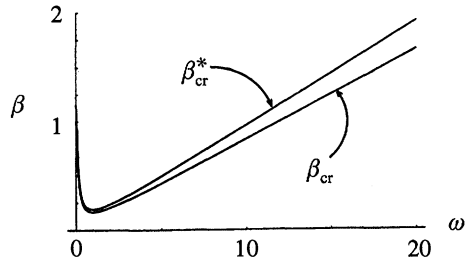

Figure 2. Critical values of β above which homoclinic tangles exist.

of these rest solutions were small enough (or gone altogether) so they could be easily avoided.

The formulae for these critical values and optimal inputs simplify significantly in the small damping and high frequency limits and these correspond to the ranges in which we carry out most of the experiments and simulations. In the small damping limit, that is, for $r \sim 1$ and $\delta \sim 0$, the phase angles have the following first order values

$$\phi_j \sim \pi, \quad \nu_j \sim \tfrac{1}{2}\pi \Rightarrow \hat{\psi}_3 \sim 3\pi \tag{25}$$

which implies that in the input acceleration, the third harmonic should be out of phase with respect to the first harmonic. This has some interesting consequences as described below. For small damping, the amplitude ratio of the third to first harmonics for the optimal input is given by

$$\gamma_3/\beta \sim 1 + 9\omega^2/[18(1+\omega^2)] \tag{26}$$

which approaches the simple value of $\frac{1}{2}$ for large values of ω. Therefore, for small damping and high frequency excitation, if one is near the bifurcation boundary, to have the best hope of untangling the manifolds one should add to the input acceleration a third harmonic which has half the amplitude of the primary harmonic and should be out of phase with it.

An example case is shown considered with $\delta = 0.03$, $r = 0.95$, and $\omega = 1.0$. For the excitation levels considered, which are very near the critical values, there exist two quite robust attractors, one confined to each potential well, and no stable steady-states exist which cross from side to side. We consider a grid of initial conditions in Σ and make a coded map which indicates the side at which each point in the grid ends up impacting a steady-state, white indicating motions which end impacting at $x = +1$ and black indicating those which end at $x = -1$. This shows the basins of attraction for the two attractors and their boundary is the basin boundary. Figure 3*a* shows the result for $\beta = 0.125$, $\gamma_3 = 0$, i.e. only a single harmonic input with amplitude a little above the critical value $\beta_{cr} = 0.1112$. The excitation and the resulting separation function $d(t_0)$ are shown in figure 4. Figure 3*b* shows a blow-up of a very small region of that shown in figure 3*a*, demonstrating the fractal nature of the boundary between black and white. When a third harmonic with $\gamma_3 = 0.03476$, $\psi_3 = 3.065$ (the optimal values for this case) is added to the excitation, the basins of attraction given in figure 3*c* result, with a blow-up shown in figure 3*d*. The corresponding input and $d(t_0)$ are depicted in figure 4. The addition of the third harmonic has destroyed the fractal nature of the basin boundary (although the gross features of basin boundaries persist). A potentially more important consequence of this added harmonic is that as the manifolds no longer intersect, no steady-state cross-well motions, periodic or chaotic, can exist.

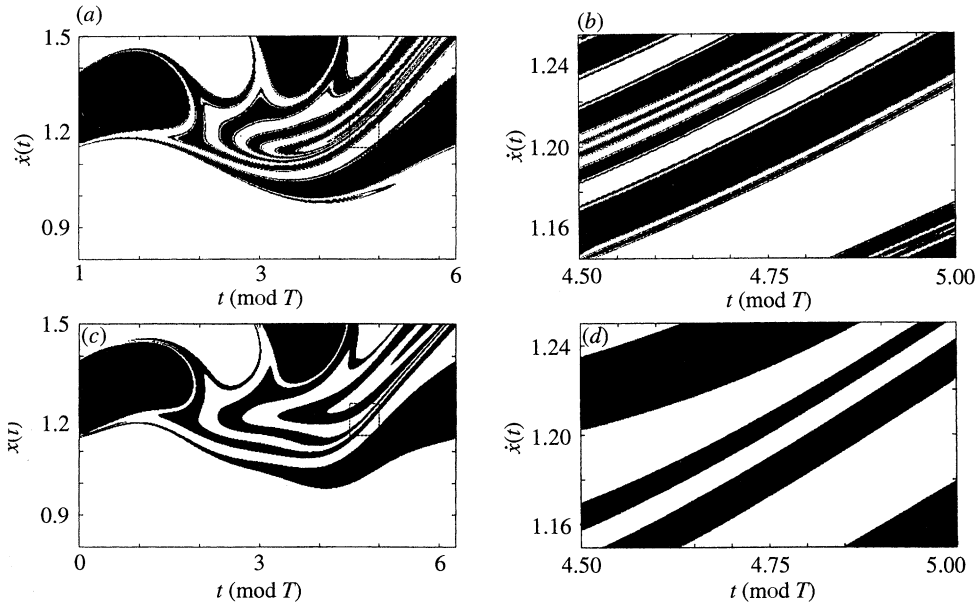

Figure 3. (*a*) Basins of attraction for the single harmonic input. (*b*) Blow-up of small region showing fractal nature. (*c*) Basins of attraction for the single plus optimal third harmonic. (*d*) Blow-up of small region.

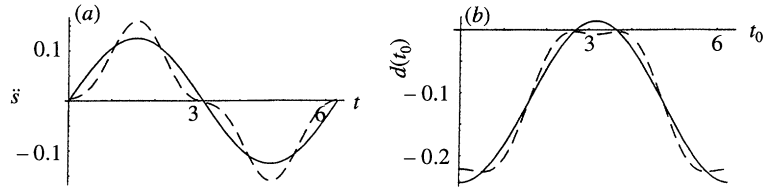

Figure 4. (*a*) Acceleration input: ——, single harmonic case; – – –, single plus optimal third harmonic. (*b*) Separation function: ——, single harmonic case; – – –, single plus optimal third harmonic.

It is of interest to note that the acceleration input of figure 4*a*, with the added third harmonic that destroys the fractal nature of the basin boundaries, has a higher peak value than that for the single harmonic case. This results from the way the phases of the various harmonics are mapped from the excitation to the separation function.

(*b*) *Experiments*

The analysis presented above provides a boundary in parameter space which separates regions in which cross-well chaos can and cannot occur. (The theory says nothing about chaotic motions which repeatedly bounce on the same side and these have been observed experimentally; see Moore & Shaw 1990.) We experimentally investigated the effect of the excitation amplitude and frequency on the threshold at which cross-well chaos could occur. The details of the experimental apparatus and the procedures used can be found in the Appendix. In measuring the threshold of cross-well chaos, we had to overcome the practical problem of deciding when such chaos occurred in a sustained manner. This problem arises because as one approaches the threshold by decreasing the excitation amplitude, the number of crossings decreases as expected, but it is impossible to ensure that the system will never cross.

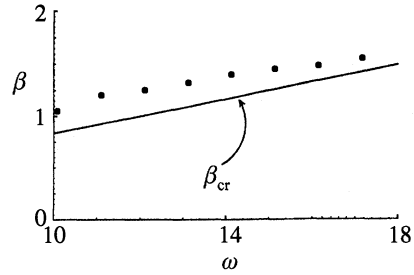

Figure 5. Thresholds for steady-state chaos: curve is theory (equation 22), dots are experimental values.

Table 1. *Experimentally determined threshold for cross-well chaos*

forcing frequency, ω/Hz	β_{cr}	forcing frequency, ω/Hz	β_{cr}
10 (10.1)	1.05	11 (11.1)	1.20
12 (12.1)	1.25	13 (13.1)	1.32
14 (14.1)	1.40	15 (15.1)	1.45
16 (16.1)	1.48	17 (17.1)	1.55

Our solution was to complete three runs, each of 4500 forcing cycles beyond an initial phase during which transients died out, and if any run had more than three crossings it was deemed to be above the threshold. Because of the co-existence of many different solutions (in some cases even a rest solution) these boundaries were ascertained from 'above', i.e. we first ensured we had a chaotic response at a relatively high β value and then, over a number of runs, reduced the β value until our criterion was no longer met. This was done for several values of ω. Such a criterion gives a bound which is somewhat above the actual threshold (in terms of β) as there can be no steady-state crossings below the threshold. This is indeed reflected in our results, which are given in table 1 and figure 5. Figure 5 shows the analytically predicted threshold as a solid line and the experimental data as dots. It is seen that the predicted boundary is quite close to the actual one and that a less conservative criterion used in the experiments would slightly lower the experimental data, improving the agreement. The reason that the Melnikov criterion works much better in this case than in others, say for Duffing's equation (see Moon 1992), is that this system is undergoing single-well chaos just below the boundary over a wide range of frequencies. Thus, as the boundary is crossed by increasing β, the response of the system can immediately start to 'leak' from one side to the other. The rate at which the system does so is the topic of the following section.

To appreciate the form of the cross-well chaotic responses observed when $\beta > \beta_{cr}$, see figure 6. Figure 6*a* represents the angular displacement of the pendulum over a time interval of 50 s. It was obtained at an acceleration equivalent to a β value of 1.8 with a frequency of 12 Hz, that is $\omega = 12.12$ and hence, $\beta_{cr} = 1.01$. We can clearly see that a total of 29 crossings occurred in an apparently random manner during this interval. To fully appreciate the timescales involved we have re-plotted the same case over the time interval 0–2 s and have also included the associated time trace of the base acceleration. These are shown in figure 6*b*, *c* respectively. From figure 6*b* we can clearly see the impacts occurring against one of the boundaries and, near $\tau = 1.2$ s, a crossing to the other boundary.

We also investigated the effect of an added third harmonic on the threshold.

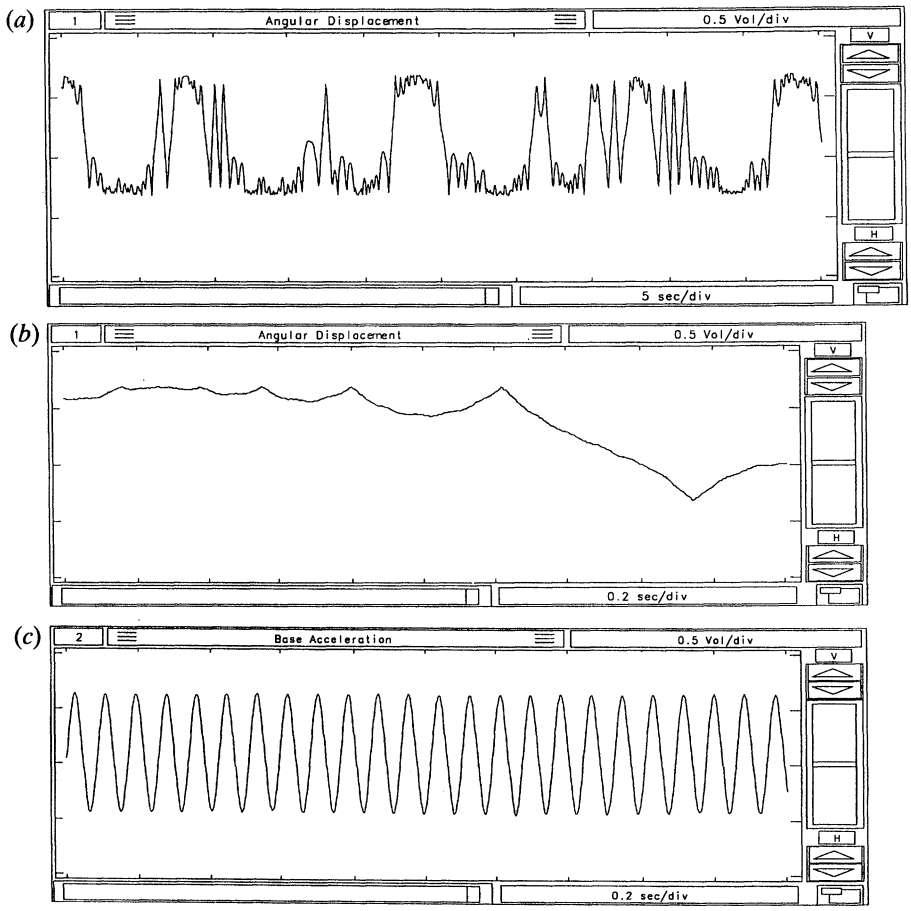

Figure 6. (*a*), (*b*) Experimental time trace of pendulum angle. (*c*) Experimental time trace base acceleration.

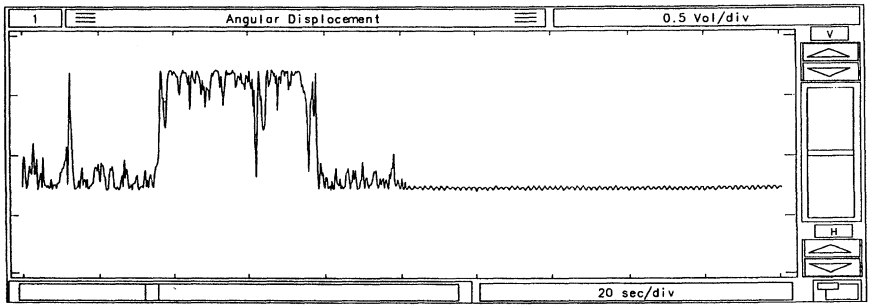

Figure 7. Experimental time trace of pendulum angle.

Surprisingly, no conclusive results were obtained when we added the optimal third harmonic. However, we did observe that if we used an optimal third harmonic added in phase instead of out of phase, then the steady state, cross-well chaos could be delayed in some cases. Indeed we encountered one dramatic example at a β value of 1.44 and $\omega = 12.12$. Figure 7 shows the angular displacement of the pendulum as it was recorded over a time interval of 200 s. At a time of 100 s an in-phase third

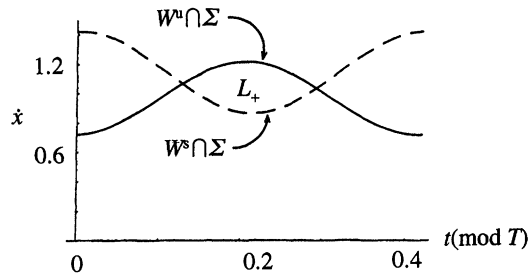

Figure 8. The stable (– – –) and unstable (——) manifolds in the Poincaré section, showing the turnstile lobe L_+. $\beta = 3.74$, $\omega = 1.50$, $r = 0.90$, $\delta = 0.03$.

harmonic of magnitude $\frac{1}{2}\beta$ was added to the base acceleration which very clearly suppressed the cross-well chaos. This result has been previously reported in Shaw (1990) at which time it was believed that an in-phase third harmonic was the optimal for extending β_{cr}. However, the analysis undertaken in this paper has shown that the out-of-phase third harmonic is optimal (in the small damping case). Nevertheless, the experimental results indicate that an in-phase third harmonic of magnitude $\frac{1}{2}\beta$ can raise the β value at which sustained cross-well chaos occurs. Although this is not directly relevant to the theory of §3 we report it here as a matter of record. This specific case is most likely due to the introduction of a stable periodic motion, or the movement of its basin of attraction, when the higher harmonic is added. Further comment on this matter is given in §5.

4. Cross-well transitions and phase space flux

We now turn our attention to some properties of steady-state cross-well chaos in this system. In particular, we would like to characterize the rate at which the system makes transitions from one side to the other. It will be shown that information in the separation function is useful for approximating this rate and that a quite coarse theory provides reliable predictive capabilities over a wide range of parameters for simple, single harmonic inputs.

The first pieces of the stable and unstable manifolds in the Poincaré section, $\dot{x}^s(t_0)$ and $\dot{x}^u(t_0)$ respectively, as computed in the previous section, play a central role in the development. These are shown in figure 8 for a particular set of parameter values. By definition, points in $\dot{x}^s(t_0)$ will approach the periodic solution as $t \to \infty$. Thus, points above $\dot{x}^s(t_0)$, after applying the impact rule and allowing free flight to the next impact, will next impact at $x = -1$, whereas points below $\dot{x}^s(t_0)$ will undergo their next impact again at $x = +1$. Similarly, points in $\dot{x}^u(t_0)$ are those that arrive at Σ from the periodic solution and thus, points above $\dot{x}^u(t_0)$ are those that have just come from an impact at $x = -1$ and points below $\dot{x}^u(t_0)$ are those that have just come from an impact at $x = +1$. Therefore, the points in Σ that lie above $\dot{x}^s(t_0)$ and below $\dot{x}^u(t_0)$ are the points that have been trapped at $x = +1$ for two successive impacts and will next impact at $x = -1$, i.e. they will make a transition. This area is a *turnstile* for the Poincaré map, $P: \Sigma \to \Sigma$; it is denoted as L_+ and is shown in figure 8. A turnstile is a piece of phase space which is transported between regions which have different qualitative features (in this case, the two potential wells). Wiggins (1992) contains very detailed descriptions of these concepts and many examples and references. The independent work of McRobie & Thompson (1992) is also directly relevant. (Note

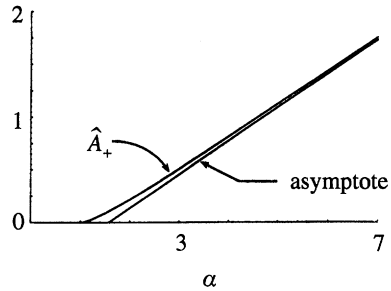

Figure 9. The area of L_+ versus $\alpha = \beta/\beta_{cr}$.

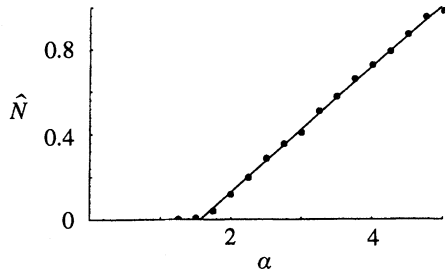

Figure 10. Normalized number of cross-well transitions against α: simulations.

that this turnstile is essentially the same as the usual one defined in Wiggins (1992) but that it appears in a different form due to the unusual map taken for this system.)

Since $d(t_0) = \dot{x}^u(t_0) - \dot{x}^s(t_0)$, the area of L_+, denoted here by A_+, is given simply by the integral of $d(t_0)$ over the time interval for which $d(t_0)$ is positive. Letting t_1, $t_2 \in [0, T)$ be the times between which $d(t_0) > 0$:

$$A_+ = \int_{t_1}^{t_2} d(t_0)\, \mathrm{d}t_0. \tag{27}$$

For a single harmonic input,

$$d(t_0) = -\tfrac{1}{2}D_0 + D_1 \sin(T_0) = \tfrac{1}{2}D_0[-1 + 2D_1 \sin(T_0)/D_0],$$

and A_+ can be computed in closed form. It is given by

$$A_+ = (D_0/\omega)\,[2 \arcsin(1/\alpha) + 2\sqrt{(\alpha^2 - 1)} - \pi], \tag{28}$$

where $\alpha = \beta/\beta_{cr} = -2D_1/D_0$, and L_+ exists only for $\alpha > 1$. For $\alpha < 1$, no cross-well chaos exists and as α increases, A_+ also increases, leading to a greater ability for the system to make transitions. For comparing simulation data with experimental data, this area is non-dimensionalized by the period of excitation, T, and the damping level, D_0, as follows:

$$\hat{A}_+(\alpha) = |A_+/(D_0\, T)| = [\sin^{-1}(1/\alpha) + \sqrt{(\alpha^2 - 1)}]/\pi - \tfrac{1}{2}. \tag{29}$$

For large values of α this is asymptotic to the line $(\alpha/\pi - \frac{1}{2})$, which crosses zero at $\alpha = \frac{1}{2}\pi$. The function $\hat{A}_+$ and its asymptote are shown in figure 9.

A number of simulations and physical experiments were carried out to determine the influence of various system parameters on the rate of transitions. These runs were carried out for extremely long times in order to obtain valid averages; 40000–50000 forcing periods were typically used. For each run, the number of times the system crossed from one side to the other was counted and labelled as N. This number was

Table 2. *Parameter values and number of crossing for simulations*
(In all cases the number of forcing cycles was $n = 50000$.)

data set	ω	r	δ	D_0	β_{cr}	β/β_{cr}	N	$\hat{N}$
1	15	0.9	0.03	−0.349	1.245	1.25*	18	0.001
						1.50*	50	0.007
						1.75*	294	0.040
						2.00	857	0.117
						2.25	1429	0.196
						2.50	2084	0.285
						2.75	2586	0.354
						3.00	2964	0.406
						3.25	3696	0.506
						3.50	4197	0.574
						3.75	4799	0.657
						4.00	5277	0.722
						4.25	5754	0.787
						4.50	6354	0.869
						4.75	6456	0.952
						5.00	7163	0.980
2	20	0.9	0.03	−0.349	1.657	3	2402	0.438
						4	3593	0.721
						5	5736	1.046
						6	6956	1.269
						7	8296	1.513
3	15	0.9	0	−0.222	0.793	2	189	0.041
						3	1475	0.317
						4	3469	0.745
						5	periodic	—
4	20	0.9	0	−0.222	1.056	2	68	0.019
						3	1303	0.373
						4	2490	0.713
						5	3913	1.121
5	15	0.9	0.10	−0.646	2.304	2	1678	0.200
						3	3963	0.473
						4	6155	0.735
						5	8791	1.049
6	20	0.9	0.10	−0.646	3.066	2	1229	0.196
						3	2955	0.470
						4	4851	0.772
						5	6755	1.075

* Not included in line fit.

then normalized by dividing it by the total number of forcing cycles, n, the period of excitation, T, and the value of D_0, yielding the average number of transitions per period normalized by the damping level: $\hat{N} = N/(nTD_0)$. (The quantity nT is simply the duration of the sample.) These values were then plotted versus $\alpha = \beta/\beta_{cr}$.

The results for simulations of the system with the experimental parameter values are shown in figure 10 and table 2 provides the parameter values and other data for this and other simulation runs. Figure 11 shows analogous data from the experiments, with table 3 showing the associated data obtained from the experimental runs. There

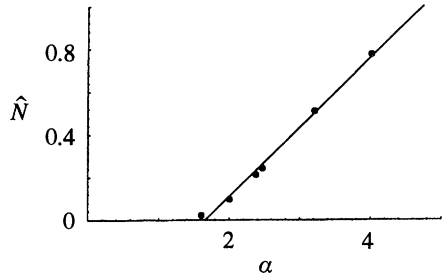

Figure 11. Normalized number of cross-well transitions against α: experiments.

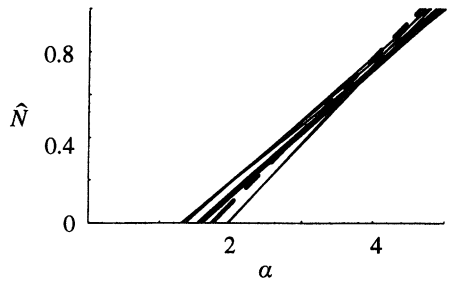

Figure 12. Least squares best-fit lines to data sets. Thin lines are for individual simulation data sets (see table 2), thick solid line is for all simulation data taken together, thick dashed line is for experimental data (see table 3 and figure 11).

Table 3. *Parameter values and number of crossing for experiments*

(In all cases the number of forcing cycles was $n = 40500$.)

data set	ω	r	δ	D_0	β_{cr}	β/β_{cr}	N	$\hat{N}$
experimental	15.1	0.9	0.03	−0.349	1.250	1.61*	120	0.020
						2.01	560	0.095
						2.38	1250	0.213
						2.47	1426	0.243
						3.21	3004	0.512
						4.02	4538	0.773

* Not included in line fit.

is very good agreement between the simulation and experimental data (this is due to the relative ease with which a reasonable mathematical model is obtained for this system). More striking is the qualitative agreement between the data and the form of the turnstile area, $\hat{A}_+$: the data and $\hat{A}_+$ are very close to linear for $\alpha > 2$, tail off to zero in the range $1 < \alpha < 2$, and no crossings are observed below $\alpha = 1$ (as must be the case).

The least-squares best fit of the data to a line was obtained for each individual data set and to the collected simulation data. (Only data for $\alpha > 2$ were used in the fits, since this is roughly the linear range.) The form for the best-fit is taken to be

$$\hat{N} = a\alpha + b \tag{30}$$

for the experiment and simulation data. Table 4 provides the a and b values for individual and collective sets of data, along with the corresponding $N = 0$ values of α (which should be near $\frac{1}{2}\pi$), and figure 12 shows the collection of the best-fit lines. Although there is some scatter in the complete data set, it is very good when

Table 4. *Results for least square fit to data sets*

	a	b	α at $\hat{N}=0$ (% error)	correlation coeff.
data set 1	0.294	−0.460	1.56 (−0.5%)	0.999
data set 2	0.269	−0.352	1.30 (−17.1%)	0.998
data set 3	0.352	−0.689	1.96 (24.6%)	0.992
data set 4	0.364	−0.719	1.31 (−16.4%)	0.999
data set 5	0.281	−0.369	1.97 (25.6%)	0.999
data set 6	0.294	−0.400	1.36 (−13.2%)	0.9997
collected simulation data sets	0.296	−0.465	1.57 (−0.2%)	0.991
experimental data set	0.342	−0.595	1.74 (10.9%)	0.9997
$\hat{A}_+$ asymptote	$1/\pi$	$-1/2$	$\pi/2$ (exact)	1

considering the simple nature of the theory and the fact that runs were carried out for various δ, r, and ω values, over which D_0 varied by a factor of roughly 3 and β_{cr} varied by a factor of roughly 4.

Note that the best-fit lines asymptote to zero transitions at α values between 1.3 and 2.0, consistent with the value of $\frac{1}{2}\pi$ predicted from the theory. For $\alpha > 2$ the relationship between $\hat{N}$ and $\hat{A}_+$ is nearly linear and is assumed to be given by

$$\hat{N}(\hat{A}_+) = a\pi(\hat{A}_+ + \tfrac{1}{2}) + b \tag{31}$$

obtained by eliminating α, where the values of a and b are from the best fit lines and are given in table 4. It is interesting to note that the slopes in this relation are roughly equal to 1, as the a values are all within 25% of $1/\pi$. This is coincidental, because, although they are directly related, $\hat{N}$ and $\hat{A}_+$ are very different quantities.

Equation (31) provides a scheme for predicting the rate at which cross-well transitions take place for this system. Given the system and input parameters one can compute β_{cr} from equation (22), and then knowing $\alpha = \beta/\beta_{cr}$ allows for the computation of $\hat{A}_+$ from equation (29). The normalized number of crossings $\hat{N}$ is then given by (31) with a and b from table 4. For a given run, the actual number of crossings encountered will be given approximately by multiplying $\hat{N}$ by the duration of the run, in terms of nT, and by D_0, which depends solely on r and δ. Thus, once a and b are determined, the rescaling allows for good estimates of the transition rate to be obtained for other parameter values.

The authors did attempt to develop a probabilistic method for predicting the crossing rate using various specific quantities from the phase space (Σ, in particular). For example, several ratios involving areas (turnstile area, the area below $\dot{x}^u(t_0)$, etc.) and times (for which $d(t_0) > 0$, for which $d(t_0) < 0, T$, etc.) were investigated. However, none correlated with the probability of crossing. In any case, such a theory would require some knowledge (or an assumption) about the distribution of points in the strange attractor over a wide range of parameter conditions. Of all measures tried, the simple turnstile area provided the best match with the data obtained from experiments and simulations.

5. Discussion

When designing inputs to suppress fractal basin boundaries the input required to yield a square wave in the separation function was seen to have a divergent Fourier series with coefficients which approach a constant value for high harmonics. As pointed out to us by Brian Feeny of Michigan State University, such an input is

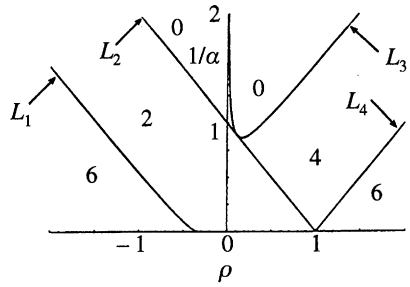

Figure 13. The number of zero crossings for $d(t_0)$, $t_0 \in [0, T)$, over a range of first and third harmonic amplitudes. Curves are given by $L_1 = -f(\rho) = -(\frac{1}{3}+\rho)^{(\frac{2}{3})}/\sqrt{\rho}$, $L_2 = 1-\rho$, $L_3 = f(\rho)$, $L_4 = \rho - 1$. Note that $\rho > 0$ corresponds to inputs and separations like the dashed curves shown in figure 4.

approaching a periodic function that has some type of impulsive behaviour superimposed on a smooth function. As this is a required input in the acceleration, it may be possible to achieve an approximation to this input by sharp impulses along with some regular harmonics, rather than the single additional harmonic used in the current study. This makes sense, as the impulsive forces would cause jumps in velocity, exactly as required for the separation function. This observation is also consistent with the fact that the optimal added third harmonic tends to sharpen the peak of the input acceleration, which in turn flattens the peaks of the separation function. It should be noted that the benefits of these additional harmonics would be incremental at best, because the separation function tends to attenuate higher harmonics, and a large part of the effect of added harmonics is achieved by the third harmonic alone.

The effects of an added third harmonic on the separation function, and thus on the nature of the lobe structure, can be summarized by writing $d(t_0)$ in normalized form as follows

$$\hat{d}(t_0) = 2d(t_0)/D_0 = -1 + \alpha[\sin(T_0) + \rho \sin(3T_0)], \tag{32}$$

where $\rho = D_3/D_1$ and we have used the fact that $\alpha = 2D_1/|D_0|$. (Here we consider only cases where the third harmonic is exactly in phase or exactly out of phase with the first harmonic in the separation function.) This function can have zero, two, four, or six zero crossings per period over the entire range of α and ρ values. By expressing the third harmonic in terms of $\sin(T_0)$ and $\sin^3(T_0)$ and studying the resulting cubic equation, a complete characterization of these features can be obtained. It is given in figure 13, which shows regions $(1/\alpha, \rho)$ space. (Note that $1/\alpha$ is used since its range is limited to $(0, 1]$.) The region over which there are no crossings reaches its lowest point in terms of $1/\alpha$, i.e. its highest in terms of α, when ρ is equal to $\frac{1}{6}$, which corresponds to the optimal solution obtained in the analysis of §3. In the region in which there are two zero crossings the waveforms are simple continuations of a simple sine wave and the 'dimples' have not yet introduced any additional zero crossings.

Several attempts were made at including the effects of a third harmonic on the transition rate and the results were inconclusive. A possible explanation for this may be the following. In the region of figure 13 labelled by 2, the area $\hat{A}_+$ given in equation (27) was numerically computed. It was found that the third harmonic does not have much influence on the area A_+ (typically less than 15% for a given amplitude of first harmonic), but the trends do indicate that the same harmonic that is able to pull the manifolds apart near the critical point, i.e. an out of phase third harmonic in the

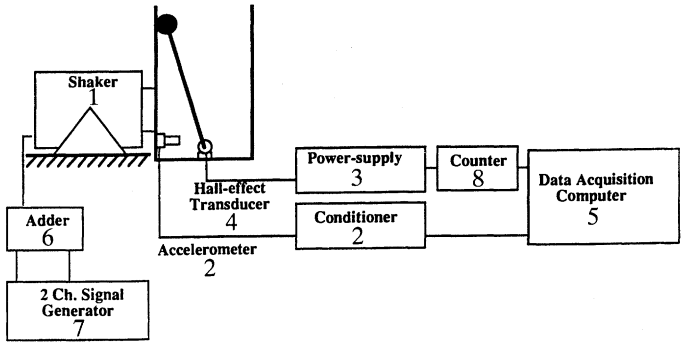

Figure 14. Schematic diagram of the experimental set-up.

acceleration, actually increases the turnstile area when one is operating above the critical point ($\alpha > 2$), thus enhancing the potential for cross-well motions. Similarly an in-phase third harmonic in the acceleration tends to discourage cross-well chaos for $\alpha > 2$ by slightly reducing A_+. Thus, for $\alpha > 2$ there is a competition between the nearness to β_{cr} and the turnstile area; increasing β_{cr} by adding a harmonic moves one closer to the threshold, but this can be offset by the larger turnstile area. These observations imply that the theory of §4 works only for simple lobe structures which arise from single harmonic inputs. The reason for this is not known. Similar considerations may also explain the observed trends in the threshold obtained experimentally for steady-state chaos, which were sometimes opposite to those expected from the theory.

It is of interest to note that the results from §4 of this paper may have application to the problem of chaotic escape from potential wells, which has several applications, including models for ship capsize (McRobie & Thompson 1993; Soliman & Thompson 1991; Falzarano *et al.* 1992). As one can estimate the rate of transitions, if the transition of interest is from a potential well to some unbounded motion, estimates of mean survival times may be obtained by computing the mean time for a single transition, which is given by setting $N = 1$ and solving for the mean survival time which is $T_s = nT|_{N=1} = [D_0(a\pi(\hat{A}_+ + \frac{1}{2}) + b)]^{-1}$. Of course, higher order statistical measures are needed if one is to develop a probabilistic method for estimating survival times. A study along these lines would be of interest.

We gratefully acknowlege support provided by grants from the U.S. National Science Foundation and the Michigan Sea Grant Program. We are also grateful to Matt Paul for carrying out some of the lengthy experimental runs.

Appendix

A schematic of the experimental set-up is shown in figure 14 and a list of the various equipment used is as follows.

1. 500 lb Electrodynamic Shaker, MB Dynamics PM500.
2. High Sensitivity Accelerometer and Associated Conditioner, PCB348A.
3. Power Supply for Item 4, HP6235A.
4. Hall-effect Angular Displacement Transducer (user designed).
5. Data Acquisition Computer, Masscomp 5550.
6. 2 to 1 Channel Signal Adder, (user designed).
7. 2 Channel Signal Generator Wavetek Model 650.
8. Counter, Philips Model PM6666.

PHILOSOPHICAL TRANSACTIONS OF THE ROYAL SOCIETY A MATHEMATICAL, PHYSICAL & ENGINEERING SCIENCES

The desired motion of the pendulum frame was generated by the electrodynamic shaker (1) which, in turn, received its signal from the two channel signal generator (7) via the adder (6). The signal generator allowed for the amplitude and phase of the third harmonic to be varied relative to its fundamental. However, the actual phase and amplitude terms encountered by the pendulum frame were measured directly using the attached accelerometer (2). The resulting angular motion of the pendulum was sensed by the Hall-effect transducer which is a non-contacting device and as such, introduced virtually no additional damping to the system. The time histories of the base acceleration and the pendulum displacements, i.e. $s''(\tau)$ and $\theta(\tau)$ respectively, were recorded using the data acquisition system (5). The counter (8) was set to count the number of times the pendulum crossed from one side to the other, in a given amount of time.

References

Falzarano, J., Shaw, S. W. & Troesch, A. 1992 Applications of modern geometric methods for dynamical systems to the problem of vessel capsizing with water-on-deck. *Int. J. Bifurcation Chaos* **2**, 101–115.

Grebogi, C., Ott, E. & Yorke, J. 1983 Crises, sudden changes in chaotic attractors, and transient chaos. *Physica* D **7**, 181–200.

Guckenheimer, J. & Holmes, P. 1986 *Nonlinear oscillations, dynamical systems, and bifurcations of vector fields*. New York: Springer-Verlag.

McRobie, F. A. & Thompson, J. M. T. 1990 Escape from potential well: lobe dynamics and organisation of invariant sets. University College London preprint.

McRobie, F. A. & Thompson, J. M. T. 1993 Criteria for escape phenomena in driven oscillators using Melnikov-like energy estimates. *Nonlinear Dynamics*. (In the press.)

Melnikov, V. K. 1963 On the stability of the center for time periodic perturbations. *Trans. Moscow Math. Soc.* **12**, 1–57.

Moon, F. C. 1992 *Chaotic and fractal dynamics: an introduction for applied scientists and engineers*. New York: Wiley.

Moore, D. & Shaw, S. 1990 Experimental response of an impacting pendulum system. *Int. J. Nonlinear Mech.* **25**, 1–16.

Ottino, J. M. 1989 *The kinematics of mixing: stretching, chaos, and transport*. Cambridge University Press.

Shaw, J. & Shaw, S. 1989 The onset of chaos in a two-degree-of-freedom impacting system. *ASME J. Appl. Mech.* **56**(1), 168–174.

Shaw, S. 1990 The suppression of chaos in periodically forced oscillators. In *Nonlinear dynamics in engineering systems* (ed. W. Schielen), 289–296. New York: Springer-Verlag.

Shaw, S. & Rand, R. 1989 The transition to chaos in a simple mechanical system. *Int. J. Nonlinear Mech.* **24**, 41–56.

Soliman, M. & Thompson, J. M. T. 1991 Transient and steady-state analysis of capsize phenomena. *Appl. Ocean Res.* **13**, 82–92.

Szemplinska-Stupnicka, W. 1992 Cross-well chaos and escape phenomena in driven oscillators. *Nonlinear Dynamics* **3**, 225–243.

Wiggins, S. 1990 *Introduction to applied nonlinear dynamical systems and chaos*. New York: Springer-Verlag.

Wiggins, S. 1992 *Chaotic transport in dynamical systems*. New York: Springer-Verlag.

PHILOSOPHICAL TRANSACTIONS OF THE ROYAL SOCIETY A MATHEMATICAL, PHYSICAL & ENGINEERING SCIENCES